SSD-TR-91-14

AEROSPACE REPORT NO.
TR-0090(5940-06)-5

A Neural Network Model of the Relativistic Electron Flux at Geosynchronous Orbit

Prepared by

H. C. KOONS and D. J. GORNEY
Space Sciences Laboratory
Laboratory Operations

10 April 1991

Prepared for

SPACE SYSTEMS DIVISION
AIR FORCE SYSTEMS COMMAND
Los Angeles Air Force Base
P. O. Box 92960
Los Angeles, CA 90009-2960

Engineering and Technology Group

THE AEROSPACE CORPORATION
El Segundo, California

This report was submitted by The Aerospace Corporation, El Segundo, CA 90245-4691, under Contract No. F04701-88-C-0089 with the Space Systems Division, P. O. Box 92960, Los Angeles, CA 90009-2960. It was reviewed and approved for The Aerospace Corporation by A. B. Christensen, Director, Space Sciences Laboratory. Lt. Tryon Fisher was the Air Force project officer for the Mission-Oriented Investigation and Experimentation (MOIE) program.

This report has been reviewed by the Public Affairs Office (PAS) and is releasable to the National Technical Information Service (NTIS). At NTIS, it will be available to the general public, including foreign nationals.

This technical report has been reviewed and is approved for publication. Publication of this report does not constitute Air Force approval of the report's findings or conclusions. It is published only for the exchange and stimulation of ideas.

TRYON FISHER, Lt, USAF
MOIE Project Offier
SSD/CLPO

JONATHAN M. EMMES, Maj, USAF
MOIE Program Manager
PL/WCO OL-AH

UNCLASSIFIED

SECURITY CLASSIFICATION OF THIS PAGE

REPORT DOCUMENTATION PAGE

1a. REPORT SECURITY CLASSIFICATION Unclassified	1b. RESTRICTIVE MARKINGS
2a. SECURITY CLASSIFICATION AUTHORITY	3. DISTRIBUTION/AVAILABILITY OF REPORT Approved for public release; distribution unlimited
2b. DECLASSIFICATION/DOWNGRADING SCHEDULE	
4. PERFORMING ORGANIZATION REPORT NUMBER(S) TR-0090(5940-06)-5	5. MONITORING ORGANIZATION REPORT NUMBER(S) SSD-TR-91-14
6a. NAME OF PERFORMING ORGANIZATION The Aerospace Corporation Laboratory Operations 6b. OFFICE SYMBOL *(If applicable)*	7a. NAME OF MONITORING ORGANIZATION Space Systems Division
6c. ADDRESS *(City, State, and ZIP Code)* El Segundo, CA 90245-4691	7b. ADDRESS *(City, State, and ZIP Code)* Los Angeles Air Force Base Los Angeles, CA 90009-2960
8a. NAME OF FUNDING/SPONSORING ORGANIZATION 8b. OFFICE SYMBOL *(If applicable)*	9. PROCUREMENT INSTRUMENT IDENTIFICATION NUMBER F4701-88-C-0089
8c. ADDRESS *(City, State, and ZIP Code)*	10. SOURCE OF FUNDING NUMBERS PROGRAM ELEMENT NO. / PROJECT NO. / TASK NO. / WORK UNIT ACCESSION NO.

11. TITLE *(Include Security Classification)*

A Neural Network Model of the Relativistic Electron Flux at Geosynchronous Orbit

12. PERSONAL AUTHOR(S)

Koons, Harry. C. and Gorney, David. J.

13a. TYPE OF REPORT	13b. TIME COVERED	14. DATE OF REPORT *(Year, Month, Day)*	15. PAGE COUNT
	FROM _____ TO _____	1991 April 10	34

16. SUPPLEMENTARY NOTATION

17. COSATI CODES			18. SUBJECT TERMS *(Continue on reverse if necessary and identify by block number)*
FIELD	GROUP	SUB-GROUP	Neural Network Relativistic Electrons Geosynchronous Orbit Space Environment Forecasting

19. ABSTRACT *(Continue on reverse if necessary and identify by block number)* A neural network has been developed to model the temporal variations of relativistic (> 3 MeV) electrons at geosynchronous orbit based on model inputs consisting of ten consecutive days of the daily sum of the planetary magnetic index ΣKp. The neural network (in essence, a nonlinear prediction filter) consists of three layers of neurons, containing 10 neurons in the input layer, 6 neurons in a hidden layer, and 1 output neuron. The output is a prediction of the daily-averaged electron flux for the tenth day. The neural network was trained using 62 days of data from 1 July 1984 through 31 August 1984 from the SEE spectrometer on the geosynchronous spacecraft 1982-019. The performance of the model was measured by comparing model outputs with measured fluxes over a 6-year period from 19 April 1982 to 4 June 1988. For the entire data set the RMS logarithmic error of the neural network is 0.76 and the average logarithmic error is 0.58. The neural network is essentially zero-biased, and for accumulation intervals of three days or longer the average logarithmic error is less than 0.1. The neural network provides results that are significantly more accurate than those from linear prediction filters. The model has been used to simulate conditions that are rarely observed in nature, such as long periods of quiet ($\Sigma Kp = 0$) and ideal impulses. It has also been used to make reasonably accurate day-ahead forecasts of the relativistic electron flux at geosynchronous orbit.

20 DISTRIBUTION/AVAILABILITY OF ABSTRACT ☒ UNCLASSIFIED/UNLIMITED ☐ SAME AS RPT. ☐ DTIC USERS	21. ABSTRACT SECURITY CLASSIFICATION Unclassified
22a. NAME OF RESPONSIBLE INDIVIDUAL	22b. TELEPHONE *(Include Area Code)* / 22c. OFFICE SYMBOL

DD FORM 1473, 84 MAR

83 APR edition may be used until exhausted.
All other editions are obsolete

SECURITY CLASSIFICATION OF THIS PAGE

UNCLASSIFIED

PREFACE

The authors thank R. Klebesadel of the Los Alamos National Laboratory, Principal Investigator for the SEE instrument, for the electron data. D. Baker and J. B. Blake generated the edited data set of daily averages used in this study. The authors would also like to acknowledge helpful discussions with M. Schulz.

CONTENTS

TABLE

FIGURES

I. INTRODUCTION

The flux of relativistic (~MeV) electrons at geosynchronous altitudes shows a strong temporal dependence on epoch relative to the onset of geomagnetic storms (Baker et al., 1979, 1986, 1987; Nagai, 1987, 1988). This electron population has attracted significant scientific attention in recent years, partly in an effort to understand the source, loss, and energization processes for magnetospheric particles generally, and partly because electrical discharges caused by these energetic particles have resulted in anomalous behavior in satellite operations in geosynchronous orbit (Reagan et al., 1983; Vampola, 1987). Quantitative modeling of the temporal behavior of the electron flux can be an important contribution toward an understanding of the basic physical processes, and also in a practical sense for use as an estimator of the electron flux when direct measurements are required but are not available. A tenable and accurate predictive technique would be an especially valuable application. Linear prediction filter techniques (e.g., Nagai, 1988) have shown considerable promise for applying time series of geomagnetic indices as proxy data for the electron flux. The linear techniques provide a simple tool for identifying the times of flux enhancements or dropouts, but they lack the ability to track the magnitude of the electron flux accurately enough for practical applications. Here we present a simple and accurate neural network model (essentially a nonlinear prediction filter) which we have used to study the physical behavior of the electrons.

The relativistic electron population at geosynchronous orbit is extremely dynamic, exhibiting flux variations of several orders of magnitude over periods of a few days. Long-term variations, including an 11-year solar cycle modulation (e.g., Baker et al., 1986) and a recurrence pattern associated with the 27-day solar synodic rotation period (Paulikas and Blake, 1979; Baker et al., 1986), have been observed as well. Notwithstanding an extensive observational data base, the origin of this electron population remains unclear. For example, it has not yet been possible to determine whether the dominant acceleration process for these electrons is internal or external to the Earth's magnetosphere. One model of the acceleration process attributes the electron energization to convective recirculation and radial diffusion of the electrons within the Earth's magnetosphere (Paulikas and Blake, 1979). A competing model ascribes the origin of the energetic electrons to initial energization within Jupiter's radiation

belts, coupled with subsequent propagation through the interplanetary medium to the Earth (Bakeret al, 1979, 1986; Nishida, 1976). The loss process for these particles is equally intriguing. It appears that if atmospheric precipitation is the dominant loss mechanism for this population, then the concomitant effects on middle-atmosphere odd-nitrogen and ozone chemistry might represent an important coupling between geomagnetic activity and climate (Baker et al., 1987; Callis and Natarajan, 1986). Clearly, much remains to be learned about source and loss processes of magnetospheric particles through further study of this electron population.

The behavior of the magnetospheric energetic electron population also has some practical significance. During extended intervals of geomagnetic activity, large fluxes of energetic electrons develop in the outer magnetosphere. These penetrating electrons can become embedded within dielectrics on satellites (e.g., printed circuit boards, cable insulation), building up electrical potentials over time which can exceed the breakdown potential of the dielectric (Meulenberg, 1976; Vampola 1987). Theoretical and experimental results (Wenaas, 1977; Beers, 1977) have shown that breakdowns occur when the fluence of penetrating electrons exceeds $\sim 10^{12}$ cm^{-2} in time periods shorter than the leakage time scales of the dielectric (typically several hours to a few days). Often, these fluence levels are exceeded in geosynchronous orbit several days after major geomagnetic storms. A quantitative forecast of the daily fluence of penetrating electrons at geosynchronous orbit would be quite valuable to the operators of these vehicles.

Superposed epoch analyses have revealed a clear, repeatable pattern in the behavior of the flux of relativistic electrons at geosynchronous orbit. Nagai (1988) showed the dependence of energetic electron flux on geomagnetic activity as measured by the *Kp* and *Dst* indices. The first feature is a rapid decrease in the flux at the onset of a geomagnetic storm. This decrease has been attributed to the combined effects of the geomagnetic field becoming highly distorted (i.e., tail-like) and the convection electric field becoming enhanced at the onset of a geomagnetic storm. The second observed feature is a flux enhancement extending from one to five days following the storm onset, and the final feature is an eventual return to "background" values about 10 days after the storm. Following the examples of several successes in the application of linear prediction filter techniques to problems in solar wind/ magnetosphere coupling (Iyemori et al., 1979; Clauer et al., 1981; Bargatze et al., 1985), Nagai (1988) produced a linear prediction model of ~MeV electron flux based on *Kp*.

Nagai (1988) related the daily sum of *Kp* (ΣKp) for 20 consecutive days to the logarithm of the average electron flux (> 2 MeV) for the 20th day. This simple linear scheme proved quite successful in reproducing the general features of the electron flux variations described above. The errors in the logarithm of the flux for this technique were less than 0.5 for about half of the days for which measurements were available. As a characteristic of the linearity of the scheme, the prediction errors tended to be largest (~one order of magnitude) for the more intense events. Since these events are of most practical and scientific interest, some effort at an improved prediction procedure is warranted.

We have taken a new approach toward modeling and forecasting the flux of energetic electrons in geosynchronous orbit based on input values of *Kp*. We have produced a neural network which successfully reproduces electron flux values based on 10 consecutive values of ΣKp. The neural network was developed using BrainMaker, neural network simulation software from California Scientific Software. Neural networks can be trained iteratively to recognize complex and nonlinear patterns in data. The neural network model provides higher accuracy than the linear techniques, especially for large events where quantitative results are of the most practical benefit. Although it is fundamentally more complex than linear prediction filters, the neural network still is simple enough to be implemented on a small personal computer. Furthermore, the neural network provides a model of the electron environment which can be used not only for predictions but also for simulation of conditions which are rarely observed in nature. Since the neural network provides an accurate representation of the response of the electron environment to geomagnetic activity, it is possible to extend the analysis eventually to study the roles of external influences (such as the solar cycle, solar wind streams, and the phase of Jupiter) on the geosynchronous energetic electron flux.

II. THE NEURAL NETWORK

The neural network used for this application consists of three layers of neurons as shown in Figure 1. The 10 neurons which comprise the first layer are connected to the input, consisting of the values of ΣKp for 10 consecutive days. A 10-day span was chosen because the impulse function obtained by Nagai [1988] from the GMS-3 electron data became essentially zero at a time lag of 10 days. Day 0 is defined to be the day for which the electron flux is calculated. The second layer of neurons, often referred to as the hidden layer, consists of six neurons. It is common to construct neural networks such that the number of hidden neurons is half the sum of the number of inputs and outputs. A single neuron is connected to the output, which represents the logarithm of the average flux of electrons for Day 0.

Connections only exist between any single neuron and the neurons in the previous layer of the network. Neurons within a given layer do not connect to each other and do not receive inputs from subsequent layers. For example , neurons in layer 1 send outputs to layer 2, and neurons in layer 2 take inputs from layer 1 and send outputs to layer 3. The connection strengths between any two layers constitute the elements of a real-valued matrix (W). The elemental values W_{ij} represent the connection strength or weight between neuron i (in one layer) to neuron j (in the next higher layer). The weight matrices are modified by training using actual data, and these matrices ultimately contain all of the information relating the input (ΣKp) to the output (the logarithm of the electron flux).

If we denote the neuron layer by a superscript, then the output, O_k^3, of the kth neuron in the third (i.e. the output) layer is related to the activation value for that neuron, A_k^3, by the transfer function:

$$O_k^3 = 1/(1 + \exp[-A_k^3]) \tag{1}$$

where

$$A_k^3 = \sum_j O_j^2 W_{jk}^{23} + T_k^3 \tag{2}$$

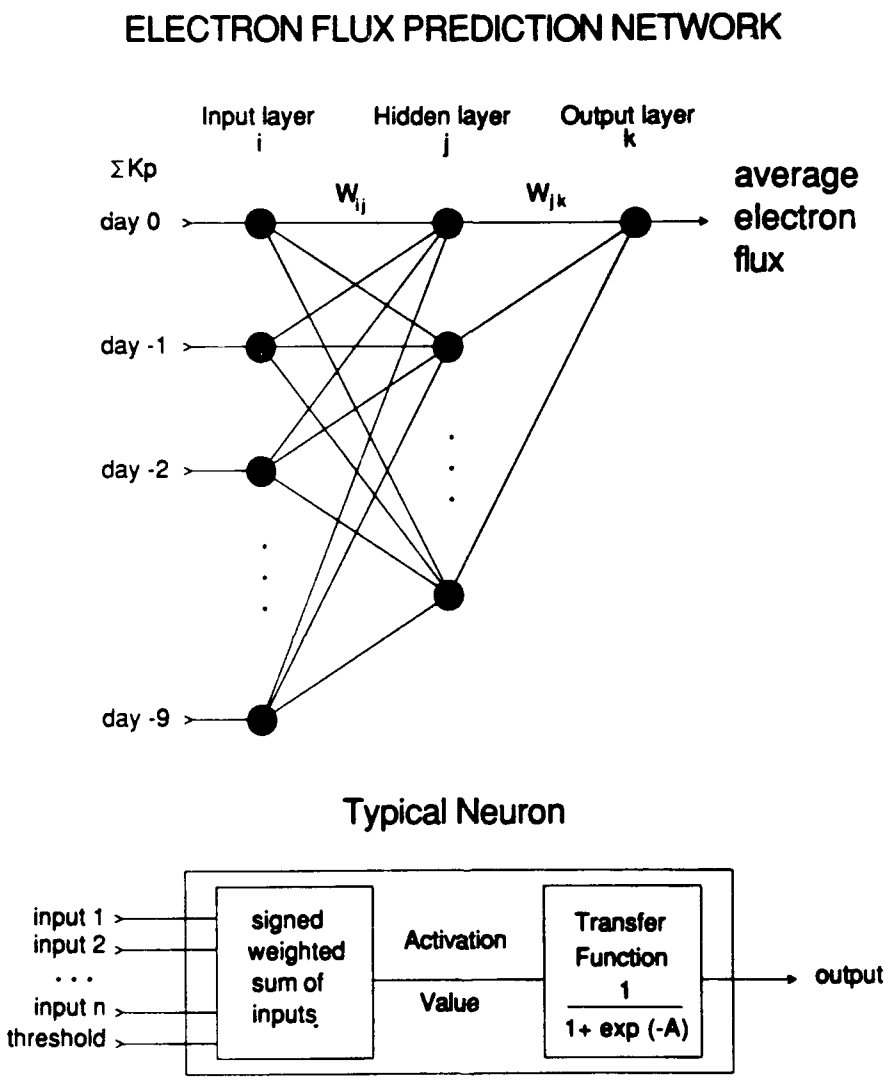

Figure 1. Diagram showing the structure of the neural network used for predicting the geosynchronous energetic electron flux based on input values of ΣKp. The values W_{ij} and W_{jk} represent weight matrices which couple input and output values to the hidden layer of neurons. The bottom diagram represents the internal function of a typical neuron.

O_j^2 is the output of the jth neuron in the second (i.e. the hidden) layer. W_{jk}^{23} is the connection strength between neuron j in the hidden layer and neuron k in the output layer, and T_k^3, is the threshold value for neuron k in the output layer. The threshold value (see Figure 1) is an additional input to a neuron that serves to normalize its output. The threshold values are calculated by the software program during network training.

Similarly

$$O_j^2 = 1/(1 + \exp[-A_j^2]) \tag{3}$$

where

$$A_k^2 = \sum_i O_i^1 W_{ij}^{12} + T_j^2 \tag{4}$$

O_i^1 is the output of the ith neuron in the first (i.e., the input) layer. W_{ij}^{12} is the connection strength between neuron i in the input layer and neuron j in the hidden layer, and T_j^2 is the threshold value for neuron j in the hidden layer.

In our model the transfer function for the neurons in the input layer is the identity function. In other words the neurons in the input layer pass their input value, I_i^1, to their output without modification. So, $O_i^1 = I_i^1$.

Since there is only one output neuron, the subscript k can be set to 1 and the output from the neural network can be written in closed form as

$$O_1^3 = 1/\left[1 + \exp\left[-\left\{\sum_j 1/\left(1 + \exp\left[-\left\{\sum_i I_i^1 W_{ij}^{12} + T_j^2\right\}\right]\right) W_{j1}^{23} + T_1^3\right\}\right]\right] \tag{5}$$

The neural network is trained using a back propagation algorithm. Back propagation is a supervised learning scheme by which a layered feedforward network is trained to become a pattern-matching engine. Training is accomplished by using sets of input/output pairs. The inputs consist of 10 known values of ΣKp and the output of one known value of the logarithm of the daily-averaged electron flux. Training uses a minimization algorithm, in this case the method of steepest descent, to minimize the error between the network output and the known

output values. The training process consists of passing many data patterns through the network in the forward direction (i .e., from input to output), then propagating the errors backwards and updating the weight matrices according to the equation

$$\Delta_p W_{ij} = \epsilon \delta_{pj} O_{pi} \tag{6}$$

where p is an index identifying the member of the training set, $\Delta_p W_{ij}$ is the change in weight W_{ij} due to training pattern p, ϵ is a constant which can be thought of as a learning rate, and δ_{pj} is given by

$$\delta_{pj} = -(\delta E_{pj}/\delta O_{pj}) F'(A_{pj}) \tag{7}$$

The error is E_{pj}, and $F'(A_{pj})$ is the slope of the transfer function that relates the output, O_{pj}, of a neuron to its activation value A_{pj}. The transfer function used in this application is a sigmoid function.

It can be shown that

$$\delta_{pj} = F'(A_{pj}) \sum_k \delta_{pk} W_{jk} \tag{8}$$

where jk refers to a weight between the hidden layer and the output layer. Thus, this provides a relationship between $\Delta_p W_{ij}$ and W_{jk} and effects the backward propagation. To initialize the training process, the network is started with completely random interconnections or weights. Training is stopped when the errors for all of the output values are within specified bounds.

The electron data discussed in this report were collected by a SEE (Spectrometer for Energetic Electrons) instrument. The SEE sensor was designed and built by the Los Alamos National Laboratory. For a description of the instrument see Baker et al. [1986]. This design has flown aboard a number of geostationary satellites. An edited data set covering the period from 19 April 1982 to 4 June 1988 from one spacecraft, 1982–019, was provided for our use. The data set consisted of daily-average count rates with background (consisting mainly of galactic cosmic rays) removed.

For this application the network was trained using count rates from the high energy ($>$ 3-MeV) electron channel. The results have been converted to flux using a geometric factor

of 0.08 and an efficiency of 0.3 for the 3-MeV channel (J. B. Blake, private communication, 1989). The training data set consisted of 62 days of data from 1 July 1984 to 31 August 1984. The training interval was selected on the basis of data continuity and the occurrence of several discrete flux enhancements within the chosen interval. In order to obtain convergence in the neural network, the training criterion was set at 10% of the complete range of output, corresponding to ± 0.5 for the logarithm of the flux or, equivalently, a factor of ~ 3. Training required 2652 passes through the 62 patterns in the training set. The 62 patterns were processed by the network in chronological order. This is not a requirement. A random order might converge more rapidly if there were systematic trends in the data. The calculations were performed on a 16-MHz Compaq Deskpro 386 personal computer in 72 minutes. Once the network is trained, many cases can be run through the network quickly by simply evaluating the functional relationship given in Eq. (5). The appropriate weight matrices and threshold neuron values are given in Table 1.

Table 1. Weight matrices (W) and neuron thresholds (T) required to evaluate the electron flux from the neural network model given by Eq. (5).

W^{12} =

2.374	-0.639	1.889	1.842	1.216	4.204
0.868	-0.264	2.198	-0.723	-1.853	-1.111
0.790	-2.876	-1.457	0.141	-2.302	-3.078
-1.060	0.605	1.482	-1.812	-2.802	2.245
-1.061	-1.293	-0.649	-0.689	-1.999	-2.245
-0.756	-0.489	2.684	-1.255	-3.711	2.609
4.986	0.369	1.885	-1.571	-2.256	-1.377
-1.358	-0.916	1.143	-1.196	-0.759	-3.052
-2.553	-0.588	-0.197	-2.524	-0.155	-0.903
-0.028	0.723	-3.071	-2.401	-2.857	1.131

T^2 =

0.818	4.236	-0.797	2.582	7.999	-1.890

W^{23} =

-2.019
1.929
2.464
4.248
-4.000
-5.139

T^3 =

0.007

III. RESULTS

The results achieved training the neural network are shown in Figure 2, which shows the predicted electron flux (ordinate) versus the measured daily-averaged flux (abscissa) for each of the 62 patterns in the training set. The plot is logarithmic on both axes, and the straight line represents a perfect correlation. The training criterion for this computation required a convergence to within 0.5 for each pattern. It should be noted that there is no a priori guarantee that a solution exists. Figure 2 shows that the specified convergence criterion was, in fact, achieved for this data set.

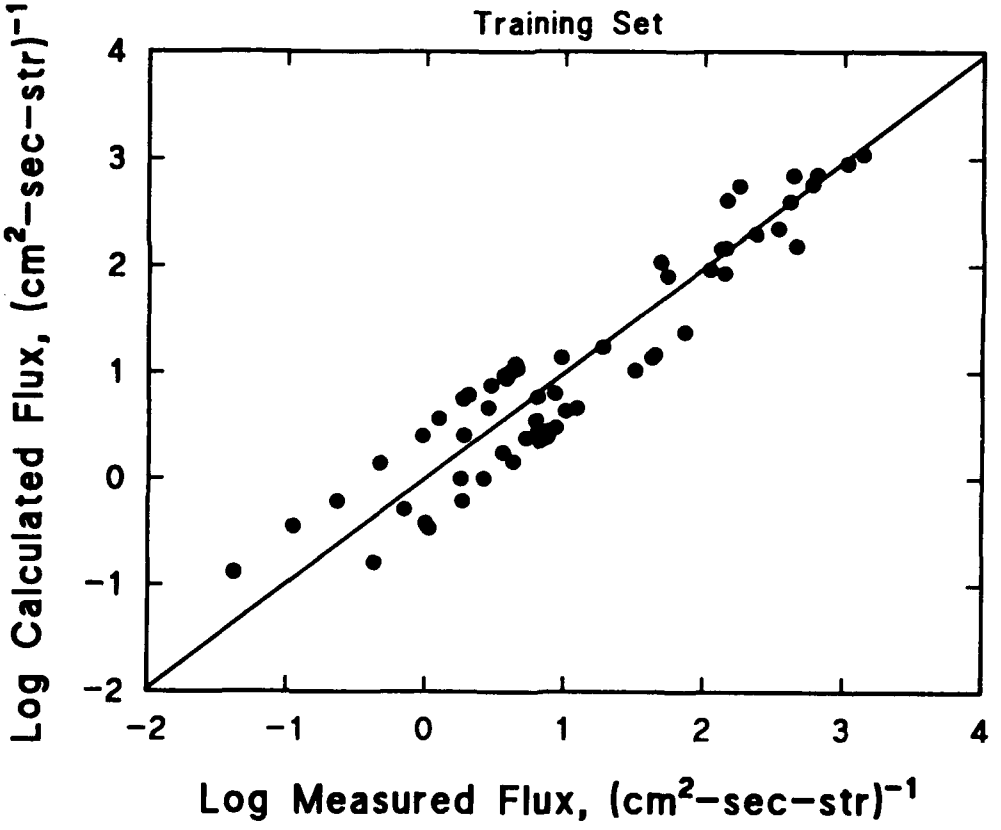

Figure 2. Plot of the predicted electron flux (ordinate) versus the measured daily-averaged flux (abscissa) for each of the 62 patterns in the training data set. The plot is logarithmic on both axes, and the heavy straight line represents a perfect correlation.

The neural network outputs for the training period are plotted together with the observed daily-averaged electron fluxes in Figure 3. The dashed line shows the observed values, and the solid line represents the neural network outputs based on 10-day input sets of ΣKp. Several large flux enhancements were observed during this period. The observed fluxes spanned a dynamic range of almost five orders of magnitude. Throughout the training interval, the maximum logarithmic prediction error is less than 0.5. Note that the key features of the temporal behavior of the data are all apparent in the neural network output, including (1) sharp flux decreases at the onsets of events, (2) fluxes which peak broadly from one to five days following the event onsets, and (3) a return to some "background" flux (not zero flux) several days after the event.

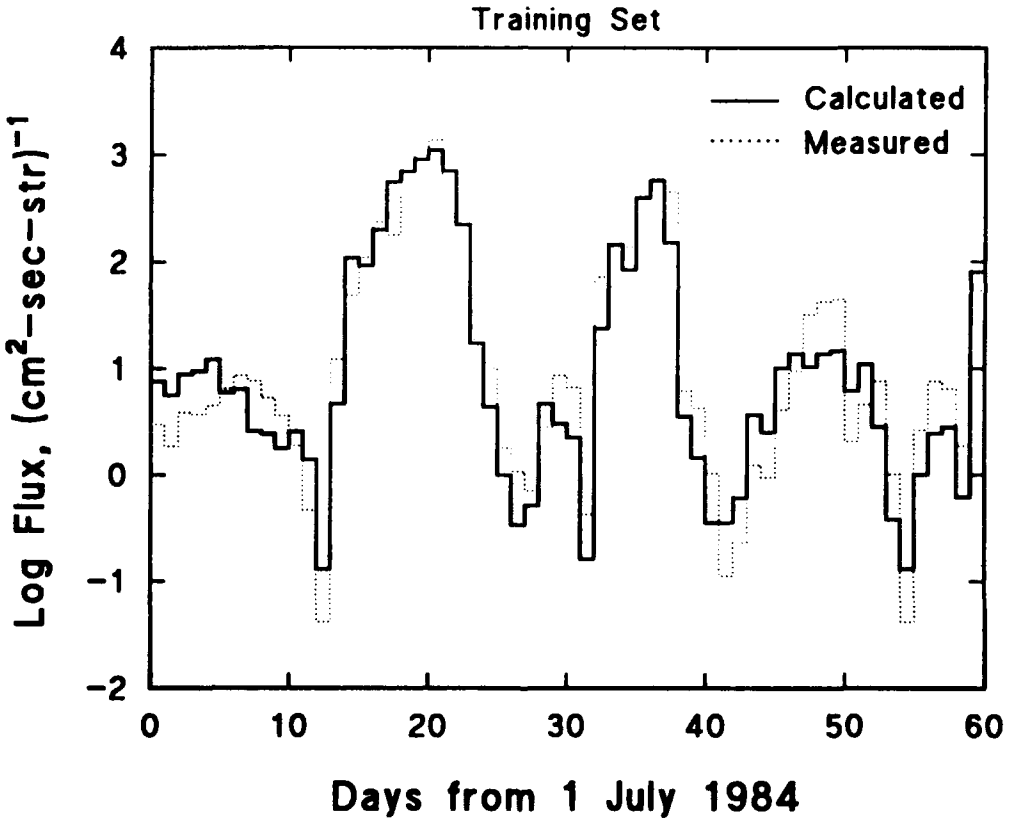

Figure 3. Plot of the neural network output (solid line) and the observed daily-averaged electron flux (dashed line) for the training period. Note that the specified convergence criterion requires that the neural network output be within ± 0.5 of the log of the observed flux for every data point in the training set.

The ability to obtain strict convergence for a lengthy set of data such as that shown in Figure 3 speaks strongly of the pattern recognition capability of the neural network technique, but the true test of a model is its ability to reproduce features which were not included in its training set. The neural network was tested by applying the trained network to all of the data, from 19 April 1982 to 4 June 1988. There are occasional gaps in the observations. Representative results from the neural network for a 60-day interval for which continuous observations are available are shown in Figure 4, along with the data. This time interval included the occurrence of three large magnetic storms, along with some extended quiet intervals. The neural network was able to reproduce the maximum flux observed after each storm quite well.

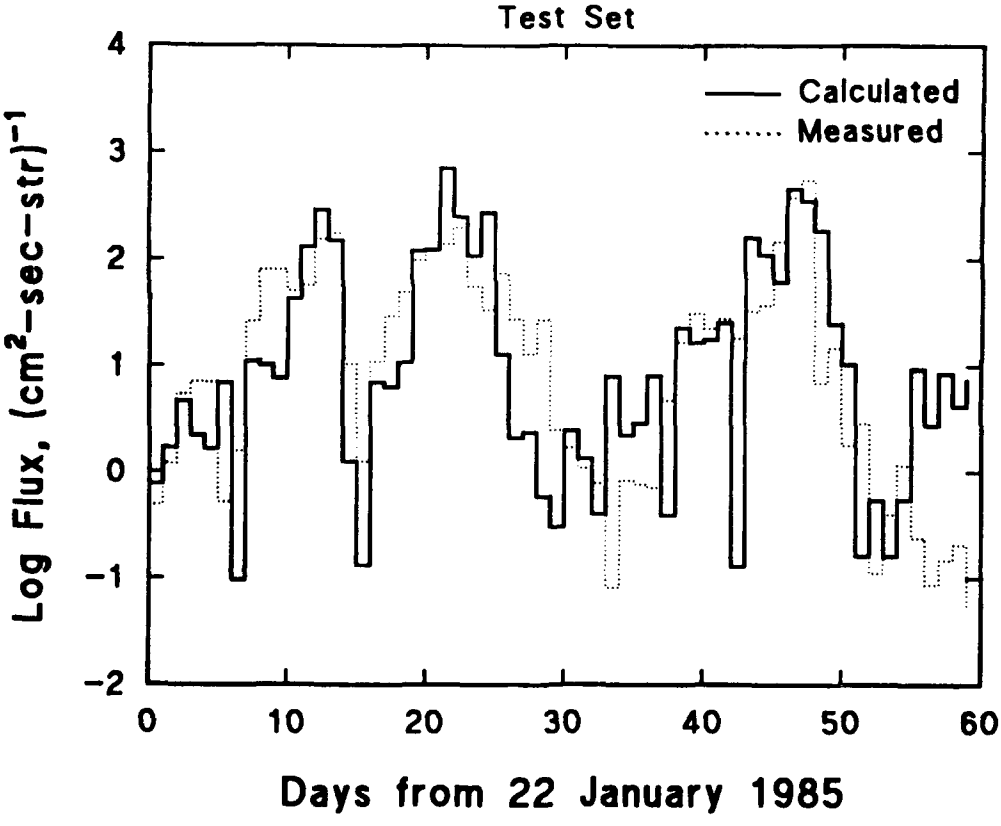

Figure 4. Plot of the neural network outputs (solid line) and measured electron fluxes (dashed line) for a 60-day interval in 1985. The plot is similar to Figure 3, but represents a period independent of the training interval for the neural network.

The overall performance of the model was measured by comparing the model outputs with measured fluxes over the entire ~six-year period from 19 April 1982 to 4 June 1988. For the entire data set, the rms logarithmic error of the neural network is 0.76 and the average logarithmic error is 0.58. An important feature of the neural network is that it is essentially zero-biased, and for accumulation intervals of several days (comparable to the time scales required to accumulate sufficient charge for the occurrence of deep dielectric discharges on satellites) the average logarithmic error is less than 0.1.

A clear strength of the neural network model is its ability to represent electron flux levels accurately during intervals of very high flux. Generally, linear prediction filters perform poorest during these sporadic intervals of high flux. A comparison of the rms error of the neural network and of a linear prediction filter (e.g., Nagai, 1988) as a function of the electron flux is shown in Figure 5. For this comparison, Nagai's original impulse function was scaled linearly to have zero offset with respect to the SEE data set. The results of Figure 5 are from the same ~six-year data set described above, but here the data set is broken down into subsets with limited ranges of flux. Note that the performance of the linear prediction filter technique degrades steadily as the flux increases, while the neural network maintains its veracity over the entire higher range of fluxes. For the largest observed events, the rms logarithmic error of the neural network model is about half that of the linear prediction scheme. This represents an actual improvement of a factor of ~5 in modeling the magnitude of the peak flux levels and accumulated fluences during large events.

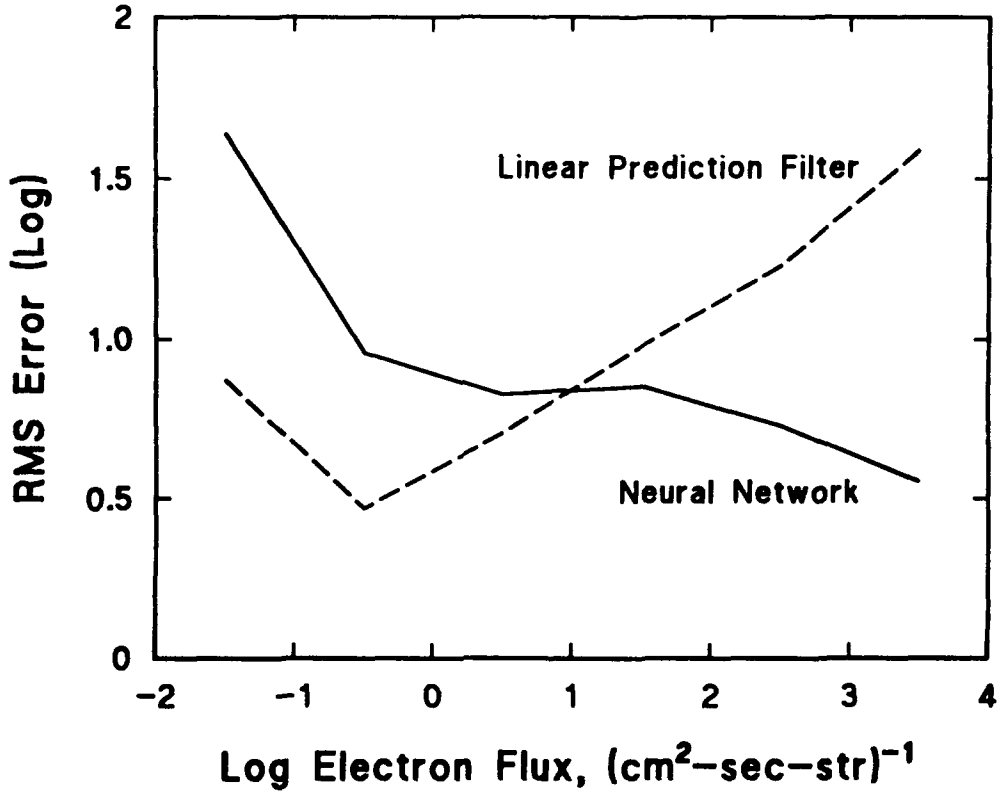

Figure 5. Comparison of the rms error of the neural network (solid line) and of a linear prediction filter (dashed line) as a function of the electron flux. Note that the performance of the linear prediction filter technique degrades steadily as the flux increases, while the neural network maintains its accuracy over the higher range of fluxes.

IV. APPLICATIONS

We have applied the neural network model to a number of interesting problems related to the relativistic flux at geosynchronous orbit. The model can be used to estimate the electron flux during time periods when satellite data are not available, as well as during periods when the electron detectors are severely contaminated by protons during solar proton events. For example, we have determined that the statistical distribution of the flux is likely to have been nearly the same over the period from 1932 to 1988 as during the period when the SEE observations were made. We have applied the model to determine the behavior of the flux during periods of prolonged steady state conditions and to isolated impulses of magnetic activity. We have also used the model to make reasonably accurate day-ahead forecasts of the electron flux. We also discuss the use of the model in determining the source of the relativistic electrons at synchronous orbit.

A. Statistics

The SEE observations that were provided to us to train and test the neural network model were from a single spacecraft and covered the six-year period from April 1982 to June 1988. The neural network model can be used with the much longer time series of ΣKp, which is available from 1932 to date, to determine the statistical behavior of the flux of relativistic electrons at geosynchronous orbit. The results, shown in Figure 6, are presented in the form of a probability distribution function; that is, the probability that the flux will exceed a given level I_0. The solid curve was obtained from the six years of SEE data. The short dashed line was obtained from the neural network model for exactly the same time period as the SEE observations. The long dashed line was obtained from the neural network model for the period from January 1, 1932 to June 30, 1988. The agreement between the probability distribution functions obtained from the neural network model for both time periods and the one obtained from the observations is remarkable. It has been hypothesized that the precipitation of relativistic electrons might have a significant effect on middle-atmosphere chemistry (Callis and Natarajan, 1986; Baker et al., 1987). This result from the neural network model implies that,

statistically, the atmospheric energy input due to relativistic electron precipitation has not varied significantly from its recent behavior over a time period of several solar cycles.

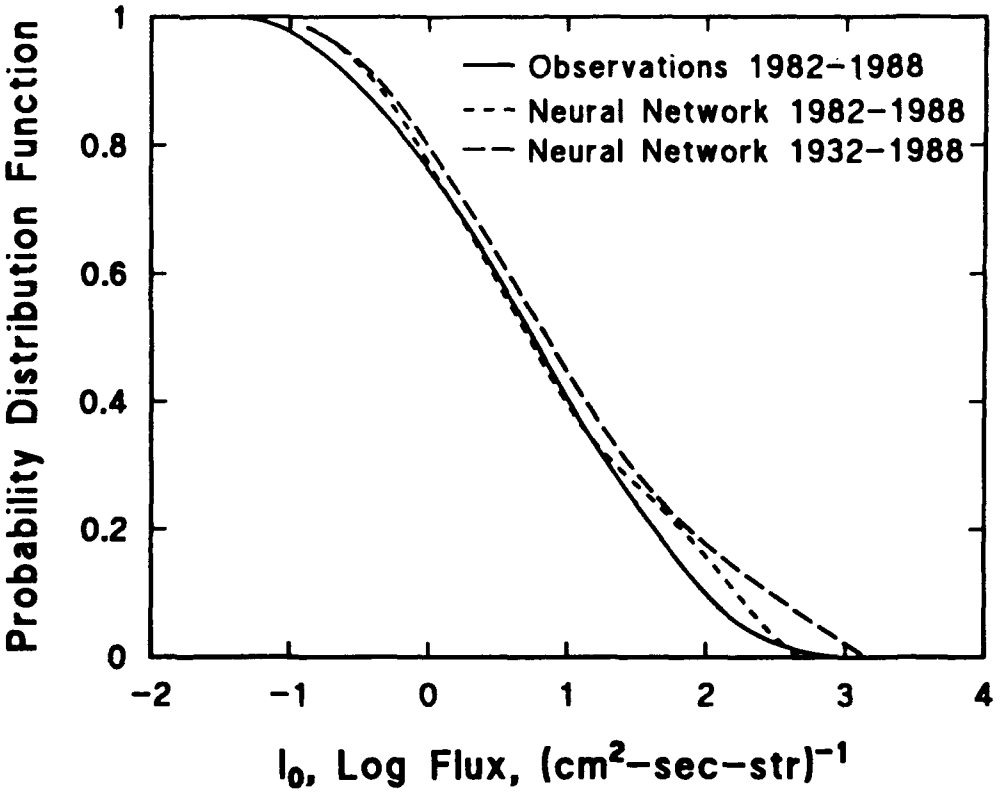

Figure 6. Probability distribution function showing the probability that the flux exceeds a specified value, I_0. SEE observations from April 19, 1982 through June 4, 1988 (solid curve); Neural network model results for the same time period (short dashed curve); Neural network model results from January 1, 1932 through June 30, 1988 (long dashed curve).

B. Steady State Conditions

The neural network can be used for simulation of conditions that are rarely observed in nature. As an example we have used it to simulate the response of the geosynchronous electron flux to prolonged steady state conditions within the magnetosphere. For this simulation, artificial inputs were constructed such that constant levels of activity were maintained for 10 consecutive days. The output plotted as the solid curve in Figure 7 represents the predicted steady-state electron flux for each (steady) level of activity.

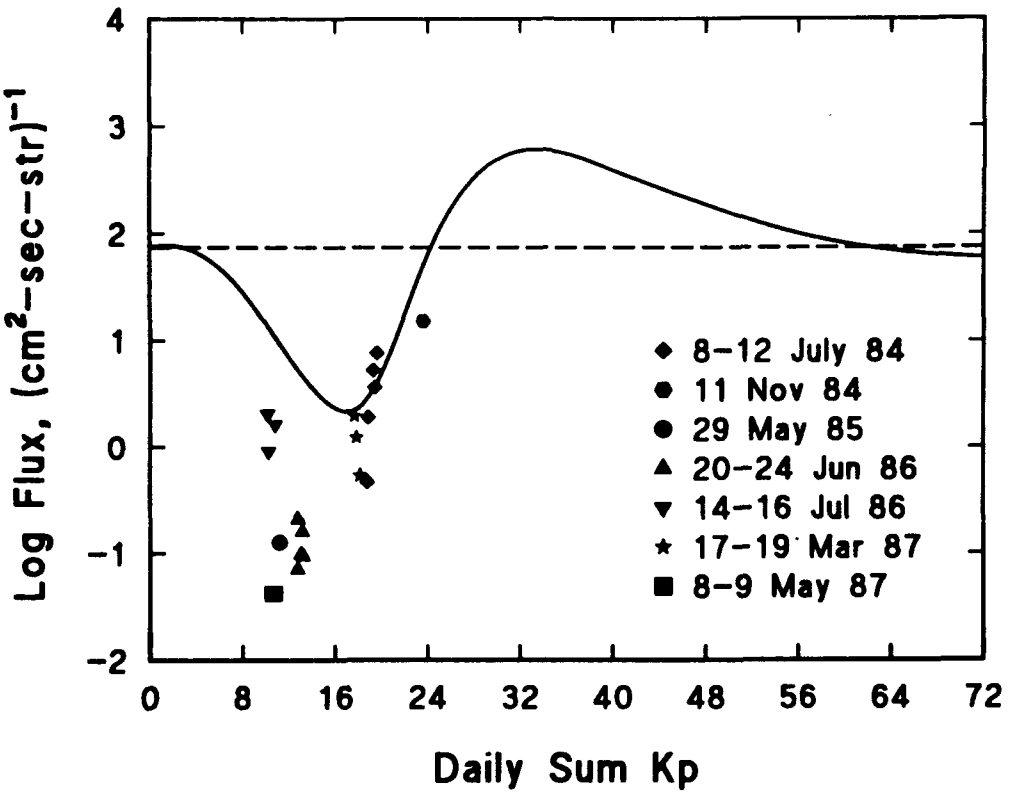

Figure 7. Plot of the results of a simulation of the response of geosynchronous electron flux to steady-state conditions within the magnetosphere. For this simulation, artificial inputs were constructed such that constant levels of activity were maintained for 10 consecutive days. The output represents the steady-state electron flux for each (steady) level of activity. Note that any linear prediction scheme would result in a straight line of positive slope on this type of display. The data points are plotted for SEE observations from periods of approximately constant ΣKp.

Exactly steady-state conditions have never been observed in the magnetosphere. In order to compare observations with the results from the model, we chose time periods for which the range of ΣKp was ± 4 about its average value for a 10-day period. During the six-year period for which SEE electron data are available, only 19 10-day periods met this criterion. The daily-average electron fluxes observed on the final day of each of these 10-day periods is plotted in Figure 7 for comparison with the model. The observations grouped around a log flux of -1 are near the noise level of the instrument. The comparison suggests that the model

is qualitatively correct, but that the actual fluxes may be lower in the range from $\Sigma Kp = 8$ to 16. Recall that the error analysis presented above showed that the accuracy of the present neural network model is relatively lower at these low fluxes.

The simulation results are intriguing and may reveal some important aspects of the nature of the source and loss of magnetospheric energetic electrons. For steadily quiet periods ($\Sigma Kp = 0$), an intermediate (i.e., nonzero) level of flux is predicted. The dashed line in Figure 7 is drawn at the log flux level corresponding to $\Sigma Kp = 0$. This feature is reminiscent of the concept of stable trapping (Kennel and Petschek, 1966) most commonly applied to the lower energy populations. At moderately higher levels of continuous activity ($\Sigma Kp \sim 16$, corresponding to three-hourly *Kp* values of 2), the predicted stable flux is diminished, indicating enhanced losses. At very high levels of activity the predicted stable flux increases toward a peak at ($\Sigma Kp \sim 32$ (corresponding to three-hourly *Kp* values of 4). The significance of the return to moderate fluxes at extremely high *Kp* values is unclear, since extreme *Kp* values were not present in the training set nor were any periods meeting our ± 4 range criterion for ΣKp present between 1982 and 1988 for ΣKp above 24.

C. Impulse Response

Figure 8, which shows the result of another set of simulated inputs, plots the flux expected following a discrete impulse of geomagnetic activity of a given amplitude. The response is plotted for an isolated impulse of geomagnetic activity on Day 0, the day for which the electron flux is calculated, and separately for an isolated impulse of activity on the preceding day. For each of these simulations, the value of ΣKp was set to zero for all days except that of the isolated impulse. Note that the model shows that the instantaneous response to an impulse of activity is a decrease of flux from the quiet steady-state value (similar to the observed flux decreases in the data). Furthermore, flux decreases monotonically with the increase in the amplitude of the impulse, resulting in very low fluxes for large impulses. Conversely, an isolated impulse of geomagnetic activity results in a monotonically larger flux for the time period one day following the impulse. The magnitude of the flux asymptotically approaches a value slightly over 4 orders of magnitude higher than that of the decrease on Day 0. These model results are similar to those features observed during large isolated storm onsets.

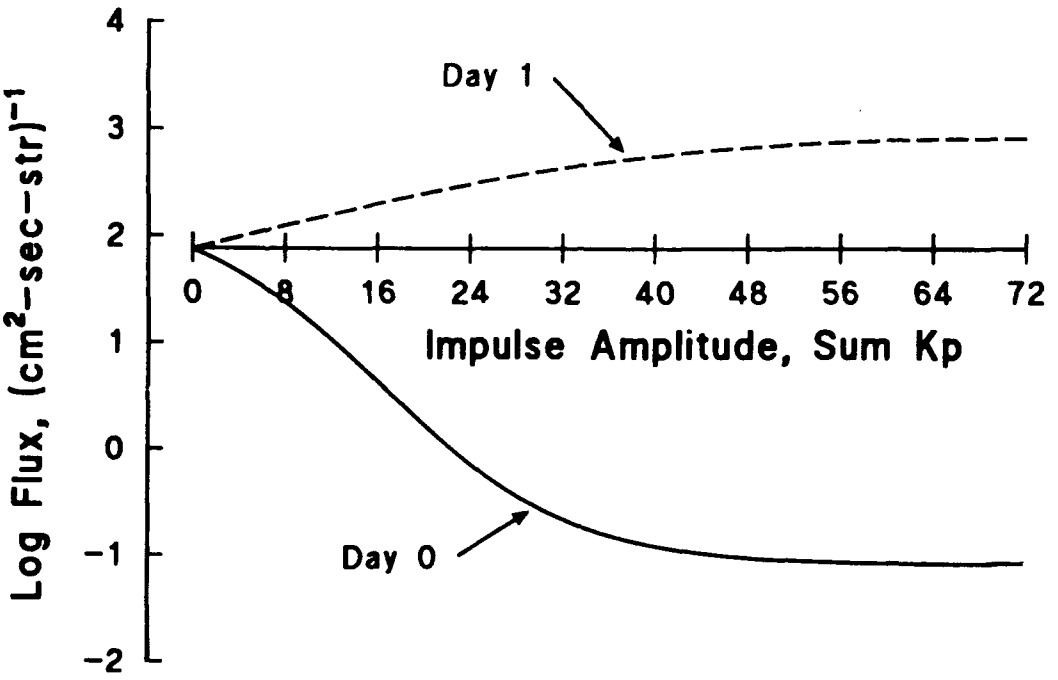

Figure 8 Plot of the fluxes resulting from an isolated impulse of geomagnetic activity occurring instantaneously (Day 0) or one day previously (Day 1). (ΣKp = 0 for all other days in the simulation period.) The plot shows the model flux as a function of the amplitude of the single impulse.

D. Forecasts

The neural network model, together with projections of ΣKp based on its historical behavior, can be used to make day-ahead forecasts of the relativistic electron flux at geosynchronous orbit. This is possible because ΣKp is not a truly random variable and because the electron flux is strongly dependent on recent (1-3 days) magnetic activity. We have examined the time series of ΣKp from 1932 to 1988, and we find that there is a strong tendency for quiet and moderately disturbed periods to persist and for violently disturbed periods to be followed by moderately disturbed periods. This behavior is shown in Figure 9 where the probability density function for ΣKp for a given day, here called Day 0, is shown parametrically for ΣKp for the previous day, Day -1. The overall probability that the value of ΣKp on Day 0 is within its

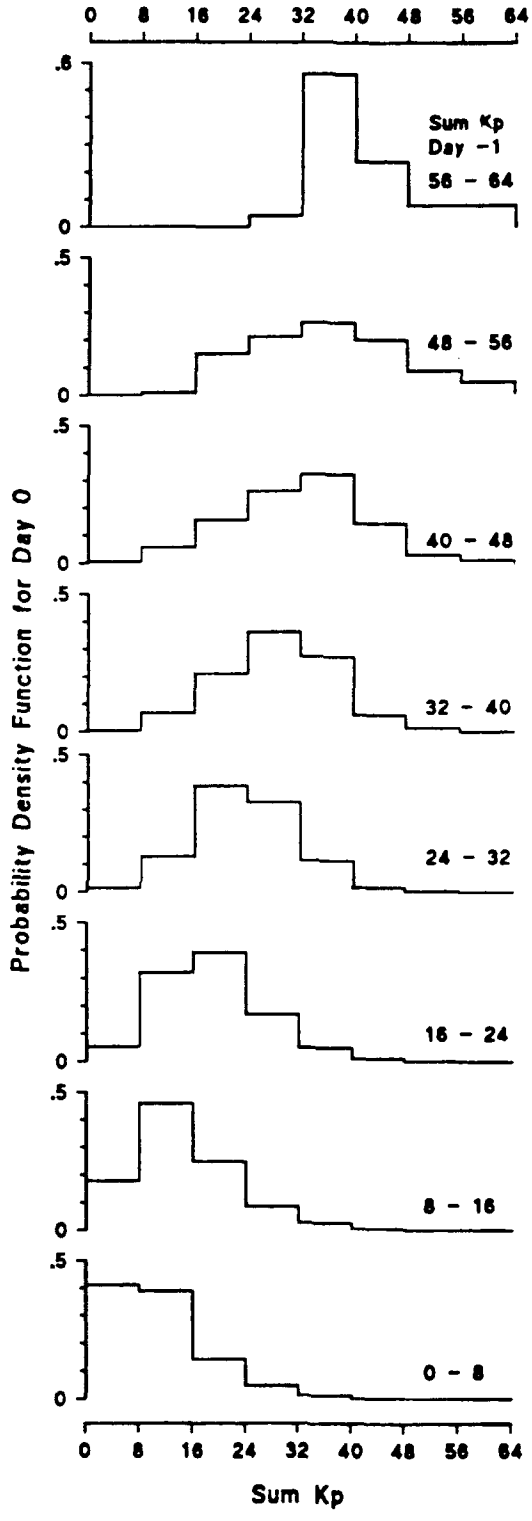

Figure 9. Probability density function for ΣKp for Day 0 plotted parametrically for eight ranges of ΣKp for the previous day, Day -1. These statistics were obtained for the period from January 1, 1932 through June 30, 1988.

most probable bin is 42%, and the overall probability that the value of ΣKp on Day 0 is within ± 1 bin of the most probable value is 86%.

Figure 10 shows a simple application of this forecasting technique to a 60-day period in early 1985. For each day a set of calculations was performed using the actual values of ΣKp for the preceding nine days and 10 values of ΣKp from 0 to 72 in steps of 8 for the day to be forecast. The three curves in Figure 10 are, in order from top to bottom, the highest forecast flux, the most probable flux (from the most probable value for ΣKp for Day 0), and the lowest forecast flux. An interesting characteristic of the forecast is that the most probable flux tends to be close to the highest forecast flux. The lowest flux is always forecast for a day on which ΣKp has its highest possible value, 72.

Figure 11 compares the flux measured by the SEE instrument for this time period with the most probable flux forecast by this technique. The agreement is excellent. In particular the most probable flux obtained from the forecast matches or slightly exceeds the measured flux at the peaks that are the times of most concern to spacecraft operators.

It is fortunate that large magnetic storms (which cannot yet be forecast) produce the lowest flux levels on the day they occur. Thus the time periods of largest error in the forecast are those of least hazard to spacecraft from the relativistic electrons. The neural network model should thus serve as a useful forecasting tool for the large flux levels that are of primary concern to spacecraft operators.

E. Jovian Electrons

A variety of observations support the suggestion that energetic electrons originating in the Jovian magnetosphere can be found in interplanetary space near Earth (Teegarden et al., 1974; Mewaldt et al., 1976). One theory for the source of electrons of similar energy in the Earth's magnetosphere ascribes their origin to initial energization within Jupiter's radiation belts, coupled with subsequent propagation through the interplanetary medium to the Earth, and their subsequent injection into the Earth's magnetosphere by magnetospheric processes (Baker et al., 1979, 1986; Nishida, 1976).

This theory postulates a modulation in the external source with a period equal to the 13-month Jovian synodic year (Chenette, 1980). However, the present neural network model

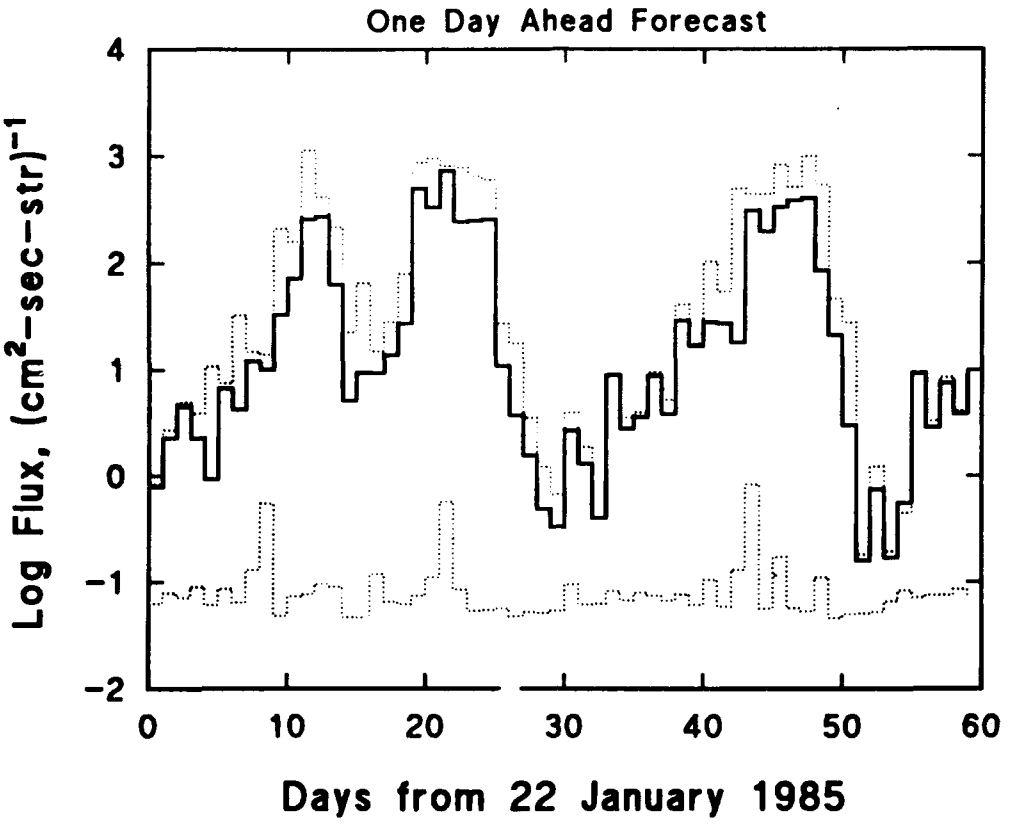

Figure 10. One-day forecasts for the electron flux for 60 days from January 22 through March 22, 1985. The top curve is plotted for the highest flux predicted. The middle curve is the flux predicted for the most probable value of ΣKp for the day of the forecast. The lower curve is the lowest flux predicted. The lowest flux normally results for ΣKp = 72 on the day of the forecast.

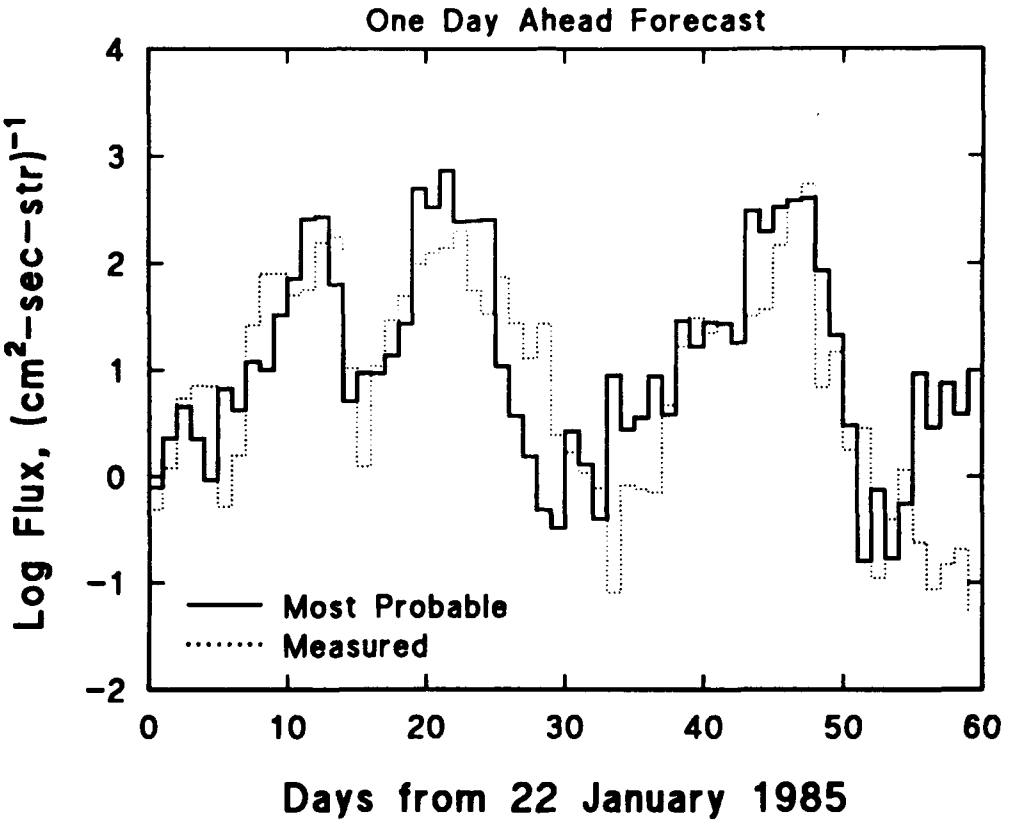

Figure 11. One-day forecasts for the electron flux for 60 days from January 22 through March 22, 1985. The solid curve is the flux predicted for the most probable value of ΣKp for the day of the forecast. The dashed curve is the flux obtained from the SEE observations.

accounts for most of the variation in the electron flux at synchronous orbit over the six-year period from 1982 to 1988 without any input representing the phase or position of Jupiter relative to Earth. This suggests that most of the variability in the flux at synchronous orbit is accounted for during this time period by internal magnetospheric processes represented in the model by ΣKp. Granted that these may be driven by external processes. However, an independent modulation of an external source related to the Jovian synodic year is not required to account for most ot the variability.

V. SUMMARY

A neural network has been developed to model the temporal variations of relativistic electron flux at geosynchronous orbit based on model inputs consisting of 10 consecutive values of the daily-summed planetary geomagnetic index, ΣKp. The neural network provides results that are significantly more accurate than linear prediction filters, thus furnishing an accurate simulation and forecasting tool for the geosynchronous electron environment.

The model can be used to infer geosynchronous electron fluxes for periods in which direct measurements are not available or are contaminated by background from solar proton events. The model has direct applicability to the analysis of satellite anomalies that are thought to be due to the deep dielectric charging process.

The neural network model provides a simple and accurate framework for studying other aspects of the behavior of the geosynchronous electron environment, including its dependence on the solar cycle and the relative phase of Jupiter. Furthermore, the model provides a capability for simulating conditions that rarely occur in nature, such as prolonged steady-state conditions or discrete impulse responses. Initial applications of the simulation capability of the neural network show that the steady state behavior of electron flux at geosynchronous orbit is complex and cannot be described by a simple linear function of ΣKp.

BIBLIOGRAPHY

Baker, D. N., P. R. Higbie, R. D. Belian, and E. W. Hones, Do Jovian electrons influence the terrestrial outer radiation zone?, *Geophys. Res. Lett., 6,* 531, 1979.

Baker, D. N., J. B. Blake, R. W. Klebesadel, and P. R., Higbie, Highly relativistic electrons in the earth's outer magnetosphere, 1. Lifetimes and temporal history 1979–1984, *J. Geophys. Res., 91,* 4265, 1986.

Baker, D. N., J. B. Blake, D. J. Gorney, P. R. Higbie, R. W. Klebesadel, and J. H. King, Highly relativistic magnetospheric electrons: A role in coupling to the middle atmosphere?, *Geophys. Res. Lett., 14,* 1027, 1987.

Bargatze, L. F., D. N. Baker, R. L. McPherron, and E. W. Hones, Magnetospheric impulsive response for many levels of geomagnetic activity, *J. Geophys. Res., 90,* 6387, 1985.

Beers, B. L., Radiation-induced signals in cables, *IEEE Trans. Nucl. Sci., NS-24,* 2429, 1977.

Callis, L. B., and M. Natarajan, The Antarctic ozone minimum: Relationship to odd nitrogen, odd chlorine, the final warming, and the eleven year solar cycle, *J. Geophys. Res., 91,* 10071, 1986.

Chenette, D. L., The propagation of Jovian electrons to Earth, *J. Geophys. Res., 85,* 2243, 1980.

Clauer, C. R., R. L. McPherron, C. Searls, and M. G. Kivelson, Solar wind control of auroral zone geomagnetic activity, *Geophys. Res. Lett., 8,* 915, 1981.

Iyemori, T., H. Maeda, and T. Kamei, Impulsive response of geomagnetic indices to interplanetary magnetic fields, *J. Geomagnet. Geoelec., 31,* 1, 1979.

Kennel, C. F., and H. E. Petschek, Limit on stably trapped particle fluxes, *J. Geophys. Res., 71,* 1, 1966.

Meulenberg, A., Jr., Evidence for a new discharge mechanism for dielectrics in plasmas, *Progress in Astronautics and Aeronautics: Spacecraft Charging by Magnetospheric Plasmas,* Volume 47, edited by A. Rosen, AIAA, New York, pp. 236–247, 1976.

Mewaldt, R. A., E. C. Stone, and R. E. Vogt, Observations of Jovian electrons at 1 AU, *J. Geophys. Res., 81,* 2397, 1976.

Nagai, T., Solar variability observed with GMS/SEM, *Papers Meteorol. Geophys., 38,* 157, 1987.

Nagai, T., Space weather forecast: Prediction of relativistic electron intensity at synchronous orbit, *Geophys. Res. Lett., 15,* 425, 1988.

Nishida, A., Outward diffusion of energetic particles from the Jovian radiation belt, *J. Geophys., Res., 81,* 1771, 1976.

Paulikas, G. A., and J. B. Blake, Effects of the solar wind on magnetospheric dynamics: Energetic electrons at geosynchronous orbit, in *Quantitative Modelling of Magnetospheric Processes*, Geophysical Monograph Series, Volume 21, edited by W. P. Olson, p. 180, American Geophysical Union, Washington, D. C., 1979.

Reagan, J. B., R. E. Meyerott, E. E. Gaines, R. W. Nightingale, P. C. Filbert, and W. L. Imhof, Space charging currents and their effects on spacecraft systems, *IEEE Trans. Electr. Insul., EI-18*, 354, 1983.

Teegarden, B. J., F. B. McDonald, J. H. Trainor, W. R. Weber, and E. C. Roelof, Interplanetary MeV electrons of Jovian origin, *J. Geophys. Res., 79*, 3615, 1974.

Vampola, A. L., Thick dielectric charging on high-altitude spacecraft, *J. Electrostatics, 20*, 21, 1987.

Wenaas, E. P., Spacecraft charging effects by the high energy natural environment, *IEEE Trans. Nucl. Sci., NS-24*, 2281-2284, 1977.

LABORATORY OPERATIONS

The Aerospace Corporation functions as an "architect-engineer" for national security projects, specializing in advanced military space systems. Providing research support, the corporation's Laboratory Operations conducts experimental and theoretical investigations that focus on the application of scientific and technical advances to such systems. Vital to the success of these investigations is the technical staff's wide-ranging expertise and its ability to stay current with new developments. This expertise is enhanced by a research program aimed at dealing with the many problems associated with rapidly evolving space systems. Contributing their capabilities to the research effort are these individual laboratories:

Aerophysics Laboratory: Launch vehicle and reentry fluid mechanics, heat transfer and flight dynamics; chemical and electric propulsion, propellant chemistry, chemical dynamics, environmental chemistry, trace detection; spacecraft structural mechanics, contamination, thermal and structural control; high temperature thermomechanics, gas kinetics and radiation; cw and pulsed chemical and excimer laser development, including chemical kinetics, spectroscopy, optical resonators, beam control, atmospheric propagation, laser effects and countermeasures.

Chemistry and Physics Laboratory: Atmospheric chemical reactions, atmospheric optics, light scattering, state-specific chemical reactions and radiative signatures of missile plumes, sensor out-of-field-of-view rejection, applied laser spectroscopy, laser chemistry, laser optoelectronics, solar cell physics, battery electrochemistry, space vacuum and radiation effects on materials, lubrication and surface phenomena, thermionic emission, photosensitive materials and detectors, atomic frequency standards, and environmental chemistry.

Electronics Research Laboratory: Microelectronics, solid-state device physics, compound semiconductors, radiation hardening; electro-optics, quantum electronics, solid-state lasers, optical propagation and communications; microwave semiconductor devices, microwave/millimeter wave measurements, diagnostics and radiometry, microwave/millimeter wave thermionic devices; atomic time and frequency standards; antennas, rf systems, electromagnetic propagation phenomena, space communication systems.

Materials Sciences Laboratory: Development of new materials: metals, alloys, ceramics, polymers and their composites, and new forms of carbon; nondestructive evaluation, component failure analysis and reliability; fracture mechanics and stress corrosion; analysis and evaluation of materials at cryogenic and elevated temperatures as well as in space and enemy-induced environments.

Space Sciences Laboratory: Magnetospheric, auroral and cosmic ray physics, wave-particle interactions, magnetospheric plasma waves; atmospheric and ionospheric physics, density and composition of the upper atmosphere, remote sensing using atmospheric radiation; solar physics, infrared astronomy, infrared signature analysis; effects of solar activity, magnetic storms and nuclear explosions on the earth's atmosphere, ionosphere and magnetosphere; effects of electromagnetic and particulate radiations on space systems; space instrumentation.